~~**An autonomously assembled octameric transmembrane helix barrel**~~

A monodisperse α-helical peptide barrel

Kozhinjampara R Mahendran[1†], Ai Niitsu[2†], Lingbing Kong[1], Andrew R Thomson[2], Richard B Sessions[3,4], Derek N Woolfson[2,3,4,*], and Hagan Bayley[1*]

[†]Contributed equally to this work

*To whom correspondence should be addressed

*e-mail: hagan.bayley@chem.ox.ac.uk; d.n.woolfson@bristol.ac.uk

[1]Department of Chemistry, University of Oxford, Chemistry Research Laboratory, Mansfield Road, Oxford, OX1 3TA, UK.

[2]School of Chemistry, Cantock's Close, University of Bristol, Bristol, BS8 1TS, UK.

[3]School of Biochemistry, Biomedical Sciences Building, University of Bristol, Bristol, BS8 1TD, UK.

[4]BrisSynBio, Life Sciences Building, Tyndall Avenue, University of Bristol, Bristol, BS8 1TQ, UK.

Abstract:

Monodisperse transmembrane barrels formed from short synthetic peptides have not been demonstrated previously. Here, we form a transmembrane pore from 35-amino-acid α-helical peptides based on the C-terminal D4 domain of the E. coli polysaccharide transporter Wza. By single-channel current recording, we define discrete assembly intermediates and show that the pore is most probably a barrel, containing eight D4 peptides arranged in parallel. We suggest that engineered α-helix barrels will find applications in nanopore technology.

The ability to engineer autonomous α-helix barrels that span membranes would add a new structural motif to the protein engineering field, and allow the incorporation of design principles garnered through studies of related water-soluble structures[1,2]. However, the construction of such systems from short peptides has been thwarted by a number of related problems. Usually, the target peptides form amphipathic helices. For water-soluble assemblies, with careful design of the hydrophobic interfaces, such helices can be assembled into discrete and defined structures[3]. However in membranes, the competing hydrophobic environment often leads to promiscuous associations, resulting in complex behaviors when peptides and lipid bilayers are mixed[2]. Nonetheless, progress is being made with the *de novo* design of small bundles of helices, notably membrane-spanning ion channels[4] and a 4-helix divalent metal-ion transporter[5], and the engineering of a dsDNA transporter based on the 12-helix ClyA pore[6]. The latter, however, is not an autonomous helix barrel in that it possesses additional structural trappings, which aid assembly[7].

To advance work in this area, we are building and engineering pores based on α helices derived both from natural examples, such as Wza[8,9], ClyA[10,11] and FraC[12], and *de novo* designs founded on the recently acquired ability to produce water-soluble barrels with up to seven α helices[2,13,14]. Here, we show that a transmembrane α-helix barrel can be built from a single 35-residue peptide. The barrel is monodisperse and most likely an octamer. The peptide is a consensus sequence derived from the D4 domains of the 340-kDa Wza polysaccharide transporters, which span the outer membranes of Gram-negative bacteria (**Fig.1a-1c)** [8], also as octamers. The peptide pore is functional; it conducts ions and binds blockers.

The redesign of membrane pores[15,16] has potential and demonstrated applications in biotechnology[17], notably in single-molecule sensing[18,19], including nucleic-acid sequencing[20,21]. Most previous engineering efforts in this area have focused on β-barrel proteins, in particular the pore formed by staphylococcal α-hemolysin[22-24]. The monodisperse barrel produced here forms the basis for a new class of structures with applications in nanopore technology.

Results

Design and biophysical properties of cWza peptide pores

The X-ray crystal structure of Wza reveals a homooctamer in which the outer-membrane-spanning D4 domain forms an α-helix barrel that comprises eight, parallel helices with the C termini oriented towards the outside of the cell[8] **(Fig. 1a,1b)**. Using SOCKET[25], we noticed that the helix-helix packing contained weak knobs-into-holes (KIH) interactions reminiscent of stable coiled-coil assemblies **(Supplementary Results, Supplementary Fig. S1)**. Therefore, we sought to test whether peptides corresponding to the D4 region could assemble autonomously in lipid bilayers to form a helix barrel. We performed a search against the non-redundant protein sequences database using BLAST (http://blast.ncbi.nlm.nih.gov/) with the *Escherichia coli* Wza D4 sequence as the query sequence. This gave 94 hits from which we derived a 35-residue consensus sequence for the D4 domain **(**cWza; **Fig. 1c)**. This cWza peptide was made by solid-phase peptide synthesis and purified by reversed-phase high-performance liquid chromatography (HPLC), **(Supplementary Fig. S2)**. Circular dichroism spectra indicated that cWza is a random coil in phosphate-buffered saline (PBS), and ~40% α-helical in PBS containing 1% n-

dodecyl β-D-maltoside (DDM) or 0.35% pentaethylene glycol monooctyl ether (C8E5) **(Supplementary Fig. S3)**. Sedimentation-equilibrium experiments by analytical ultracentrifugation showed that peptide monomers and dimers are in equilibrium, and that the monomer predominates (>90%) at a peptide concentration of 22 μM in PBS with 0.35% C8E5 **(Supplementary Fig. S3)**.

The pore-forming properties of cWza were examined by electrical recording in planar lipid bilayers. The cWza peptide spontaneously inserted into DPhPC (1,2-diphytanoyl-*sn* -glycero-3-phosphocholine) bilayers at +100 mV and multiple stepwise pore-forming events were observed **(Fig. 1d)**. Interestingly, pore formation was preceded by short bursts of transient current spikes, which we assigned as a precursor state P. The stable pores were designated as the low-conductance state L, and had a mean unitary conductance (*G*) of 0.38 ± 0.02 nS (n = 110, at +100 mV) in 1 M KCl, 10 mM HEPES, pH 7.4 **(Fig.1e, f)**. At higher applied potentials (+200 mV), the L state transformed in a sharp single step into a high-conductance state H with a mean unitary conductance of 0.97 ± 0.06 nS (n = 100) **(Fig. 1g, h)**. The pores transitioned between the L and H states at +200 mV. The durations of these states varied from several seconds to minutes and did not conform to simple exponential distributions. In most cases, the closure of L was preceded by a short current burst, which we presume to be the P state **(Fig 1i).** By contrast, the 35-residue *Escherichia coli* Wza D4 peptide (the query sequence used in the BLAST search) produced only noisy unstable pores **(Supplementary Fig. S4)**, demonstrating specificity between peptides in the cWza pore-formation process.

To probe the pore structure by site-specific chemical modification, we made cysteine mutants of cWza guided by the X-ray crystal structure of native Wza[8] **(Fig. 1b and**

Supplementary Table S1). In detergent-containing solution, these synthetic peptides behaved similarly to cWza as judged by circular dichroism spectroscopy and analytical ultracentrifugation **(Supplementary Fig. S3)**. In bilayer recordings, a mutation near the C terminus, cWza-K375C, in which the Cys side-chain was expected to point away from the pore lumen, gave similar results to the cWza peptide, except that it remained open for longer periods in the H state (G = 0.98 ± 0.06 nS, n = 100) **(Fig. 2a-2f, Supplementary Fig. S5)**. The mutant cWza-S355C, with a Cys near the N terminus and a side-chain expected to point into lumen, also gave similar results to cWza **(Supplementary Fig. S6** and **Supplementary Table S2)**. Moving further into the pore from the C-terminal side, the mutant cWza-Y373C formed less prominent P states, which nevertheless led to highly stable well-defined pores at +100 mV with a unitary conductance of 0.75 ± 0.04 nS (n = 100), assigned as the H state despite their relatively lower conductance **(Fig. 2g-j)**. The conductance of H varied linearly with the applied potential, i.e., the pore did not show rectification **(Fig. 2k)**. Two additional Cys mutants made deeper still within the pore, cWza-E369C and cWza-D366C **(Fig. 2a)**, gave noisy unstable pores **(Supplementary Table S2)**, again demonstrating specificity in the assembly process of the stable pores. We used molecular dynamics simulations to cast light on the difference between cWza and cWza-Y373C **(Supplementary Fig. S7)**. These indicated that although the cWza peptide barrel maintained its overall secondary and quaternary structure, it was dynamic and showed fraying around Y373. The cWza-Y373C peptide barrel was more stable over the simulation trajectory and its shape remained closer to the X-ray crystal structure of the D4 domain in native Wza.

Interaction of cWza peptide pores with cationic cyclodextrins

Cyclodextrins (CDs) block pores formed by native Wza[9]. Therefore, we examined the interaction of positively charged CDs with cWza peptide pores **(Supplementary Table S3)**. As noted above, both the cWza and cWza-K375C pores transition between L and H states. The octasaccharide, am_8γCD (**Fig.3a**) did not block the L states. However, it did block the H states in a voltage- and concentration-dependent manner. This behavior was examined in detail for the H state of cWza-K375C, because it remained open for longer than the H state of cWza. At positive potentials, the addition of 100 μM am_8γCD to the trans compartment (cWza-K375C was added to the cis side) resulted in transient current blockades (**Fig.3a**). Am_8γCD blocked the cWza-K375C pore completely (100% block of the open pore current), with mean dwell times (τ_{off}) of 12 ± 2 ms (n = 3) at +50 mV, and 0.12 ± 0.02 ms (n = 3) at +200 mV. The dissociation rate constant ($k_{off} = 1/\tau_{off}$) increased with increasing positive potentials, indicating dissociation by translocation **(Fig. 3a)**[9,23,24]. When the polarity was reversed, no blockades were observed. Consistent with this, the addition of am_8γCD to the cis side resulted in current blockades only at negative potentials **(Supplementary Fig. S5)**. Similar results, indicating translocation, were obtained for the smaller heptasaccharide, am_7βCD **(Supplementary Fig. S8)**. However, when the hexasaccharide, am_6αCD, was added to the trans side, k_{off} decreased with increasing voltage from +50 to +100 mV, characteristic of binding and dissociation from the same side (trans). Increases in the voltage to above +100 mV resulted in an increase in k_{off}, indicating translocation of am_6αCD through the pore **(Fig. 3b)**. In competitive binding experiments, the binding of am_6αCD and am_8γCD were readily distinguished and mutually exclusive **(Fig. 3c** and **Supplementary Fig. S9)**. Importantly, native Wza (open forms of the *Escherichia coli* Wza pore[9]) is also blocked by am_8γCD (~60% block), but the nature of the blockades differs from that of

the cWza peptide pores (100% block) **(Supplementary Fig. S10)**[9,26]. However in both cases, the dissociation rate k_{off} increases with increasing positive potentials, indicating the prevalence of translocation events.

In the case of cWza-Y373C, which exhibited a stable H state, the addition of am_8γCD to the trans compartment produced current blockades: τ_{off} = 11 ± 2 ms, at + 50 mV (n = 3) and 125 ± 25 ms, at + 100 mV (n = 3) **(Fig. 3d)**. The dissociation rate constant (k_{off}) decreased with increasing potential, indicating binding and dissociation from the same side (trans) **(Supplementary Fig. S7)**. Similar results were obtained for am_6αCD **(Fig.3d** and **Supplementary Fig. S11)**.

Subunit composition and orientation of the peptide pores in the lipid bilayer

To determine the number and orientation of the peptides in the cWza pores, we modified the Cys side-chains of cWza-Y373C *in situ* with sulfhydryl-directed polyethylene glycol reagents (MePEG-OPSS, monomethoxypoly(ethylene glycol)-*o*-pyridyl disulfide). After the formation of a single cWza-Y373C pore, 1 mM mPEG-OPSS-5k was added to the trans compartment, resulting in a single-step closure of the pore within 10 to 15 min **(Fig. 4a)**. The pore re-opened in ~2 min upon the addition of 10 mM dithiothreitol (DTT), also to the trans side (n = 10) **(Fig. 4b)**. In contrast, application of the PEG reagent to the cis side failed to close the pore (monitored for >1 h, n = 10) **(Fig. 4c)**. However, the subsequent addition of mPEG-OPSS-5k to the trans side of a pore, treated first from the cis compartment, gave a single-step closure **(Supplementary Fig. S12)**, which again re-opened in ~2 min after the addition of 10 mM DTT (trans). These data suggest that the Cys side chains — which are located towards the C-terminal end of the cWza-Y373C peptide — are all exposed on the trans side of the lipid bilayer **(Fig. 4d)**. This parallel arrangement

resembles that in the D4 domain of native Wza in the *Escherichia coli* outer membrane in which the C termini all face the extracellular medium[8,9].

Our next experiments probed the number and orientation of the peptides more precisely with the less-bulky reagent, mPEG-OPSS-1k. In this case, the addition of 1 mM PEG reagent to the trans side of the pore resulted in a stepwise decrease in current over 15 to 20 min (n = 16) **(Fig. 4e).** The pore re-opened in ~5 min after the addition of 10 mM DTT to the trans compartment. A histogram of the current steps revealed a distribution of 1 to 8 steps per experiment, but no more than eight, with 75% in the range 6 to 8 **(Fig. 4e** and **Supplementary Fig. S12)**. The sharp cut-off at 8 in the histogram displaying the number of steps suggests that the pore formed by cWza-Y373C most likely comprises 8 subunits. The addition of 1 mM mPEG-OPSS-1k to the cis side produced almost complete closure of the pore in one or two steps over 10 to 15 min **(Fig. 4f)** (n = 10). Again, the pore re-opened in ~5 min when DTT was added to the trans compartment. We speculate that the cWza-Y373C pore can only accommodate up to two 1 kDa PEG molecules added from the cis side. One end of each polymer chain must traverse the pore to reach a Cys residue on the trans side, while the remainder of the chain remains within the pore and in the cis compartment, producing a substantial current block.

These results suggest that the cWza peptides enter the bilayer C terminus first, although more circuitous assembly pathways are possible. To test the C-terminus-first route, we made additional peptides. cWza-Y373C was extended with positively charged, tetralysine (K4) tails to give peptides with: (i) a K4 tail at the N terminus, K4-cWza-Y373C; (ii) a K4 tail at the C terminus, cWza-Y373C-K4; and (iii) tails at

both termini, K4-cWza-Y373C-K4. Only K4-cWza-Y373C formed a stable pore, which had a mean unitary conductance of 0.72 ± 0.05 nS, at +100 mV (n = 50), similar to that of cWza-Y373C **(Fig. 4g)**. By contrast, cWza-Y373C-K4 formed noisy unstable pores **(Fig. 4h)**, and K4-cWza-Y373C-K4 did not show any pore-forming activity throughout 30 min of recordings **(Supplementary Fig. S13)**. These measurements are consistent with the C termini of the active cWza peptides entering first, translocating across the membrane, and the N termini remaining on the cis side.

Construction of a cyclodextrin-templated cWza barrel

As a final test of our model for the insertion and assembly of cWza, we made disulfide linked peptide-γ-cyclodextrin conjugates **(Fig. 5a)**. An activated γ-cyclodextrin harboring eight pyridyldithiol groups, $(PDPam)_8$γCD **(Fig. 5a, Supplementary Fig. S14** and **S15)**, was reacted with either cWza-S355C or cWza-Y373C in excess. As revealed by SDS-polyacrylamide gel electrophoresis, ladders of adducts were produced with estimated molecular masses (based on denatured protein standards) in the range 4 to 20 kDa for cWza-Y373C and 4 to 34 kDa for cWza-S355C **(Supplementary Fig. S15** and **Fig. 5b)**. The conjugates were extracted from individual gel bands and examined by planar bilayer recordings.

Experiments with the cWza-Y373C conjugates gave inconsistent results **(Supplementary Fig. S15).** Therefore, we focused on the cWza-S355C conjugates **(Fig. 5b)**. Only the most slowly migrating cWza-S355C conjugate, ~34 kDa, formed pores, and these were of low conductance, 0.07 ± 0.02 nS (n = 25) **(Fig. 5c)**. Treatment of these small pores with 10 mM DTT (cis) for ~10 min, rendered stable well-defined pores of unitary conductance 0.60 ± 0.05 nS (n = 25) **(Fig. 5d and Supplementary Fig. S16)**. We assume that the DTT cleaved the disulfide bonds

between the peptides and the γCD, releasing the latter, leaving a functional pre-formed pore that resembles the H state. Accordingly, the released pore was blocked reversibly by 100 μM am_8γCD from the trans compartment **(Supplementary Fig. S16)**. The H state is of consistently lower conductance than that formed directly by the cWza-S355C peptide. Therefore, we speculate that the structure of this H state differs slightly, but is kinetically stable. Notably, the protein extracted from the other bands (4, 12, 25, 30 kDa) produced only unstable noisy pores (**Supplementary Fig. S16)**. Of the two types of CD conjugate, only that built from cWza-S355C peptides has free C termini for unfettered insertion into the membrane. Thus, again, these data are consistent with an all-parallel, C-terminus-first assembly mechanism.

Discussion

Monodisperse transmembrane barrels have not been produced previously from autonomous α-helices. The outer-membrane-spanning domain (D4) of the bacterial polysaccharide transporter is an eight α-helix barrel. The structure is not buttressed by surrounding helices[27,28] and it partially resembles coiled-coil-based α-helix barrels[3,8]. Accordingly, we asked whether cWza peptides based on a consensus sequence corresponding to the D4 domain could by themselves form monodisperse transmembrane pores. Indeed they can. The barrels are most likely octamers and they are functional, conducting ions and binding cyclodextrin blockers.

We synthesized a series of 35-residue peptides and measured their membrane activities by single-channel electrical recordings. First monomeric peptides, M, or perhaps small oligomers, assemble on the bilayer leading to a precursor state, P. The P state is of very low conductance and displays a characteristic noisy current.

To our knowledge, it is the first clear example of a pore precursor formed during the membrane insertion of amphipathic α helices. The appearance of the P state is a prerequisite for the formation of stable pores, which take two forms: a low-conductance state, L, which is formed from P at low applied membrane potentials; and a high-conductance state H, which is formed from L at higher potentials. Based on these findings, we propose an assembly pathway for cWza peptides in lipid bilayers: M $\Leftrightarrow$ P $\Leftrightarrow$ L $\Leftrightarrow$ H **(Fig. 6)**. The stoichiometry of the H state is based on the counting of subunits by chemical modification during electrical recording, which reflects that of the D4 domain in the X-ray structure of native Wza[8,29] **(Fig. 1a, 1b)**. By supposing that the lumen of D4 is an electrolyte-filled cylinder (diameter 17Å, length 38Å)[8] and using a value of 10 Ωcm for the resistivity of 1 M KCl, we calculated the conductance of H to be 1.4 nS, after applying the correction of Smart et al.[30], which is consistent with our experimental value of ~0.97 nS, given the approximations used in this approach. Geometrical constraints dictate that the lower conductance of L involves both a narrowing and a lengthening of the pore, which in turn requires a decrease (relative to H) of the angle of tilt of the helices with respect to the membrane normal, as proposed for the closure of mechanosensitive channels[31-33]. To construct a model for L, the state was assumed to be a coiled-coil octamer with more-extensive knobs-into-holes interactions than found in the X-ray crystal structure of Wza[2,8]. The Crick parameters for this structure were optimized by using a genetic algorithm[2] **(Fig. 6** and **Supplementary Fig. S1)**. The relative unitary conductance values for H and L were calculated by assuming that the internal volume of L is also approximated by a cylinder (diameter 11Å, length 45Å), which gave the corrected conductance of the L state as 33% of that of the H state, by comparison with the experimental value of 40%. In addition, the unitary conductance

values for H and L were calculated by using HOLE, again yielding a value for L (0.40 nS) of 33% of that of H (1.2 nS)[30]. Many, if not all, pore-forming proteins including staphylococcal α-hemolysin assemble through prepore intermediates[7,34-38]. We have learned here that cWza, and perhaps similar amphipathic helical peptides, are likely to assemble into pores through a similar pathway **(Fig. 1e, 2b, Fig. 6, Supplementary Fig. S17).**

The L state is blocked by small molecules, for example tris(2-aminoethyl)amine **(Supplementary Fig. S18)**, whereas the H state accommodates both small molecules and larger molecules, such as cyclodextrins[23,24,39]. Moreover, the 8-fold symmetric cationic cyclic octasaccharide, am_8γCD, blocks the H state effectively **(Supplementary Table S3)**. This result and the X-ray crystal structure of native Wza support the idea that the H state is most likely an 8-α-helix barrel. Therefore, the L state, which undergoes rapid transitions into the H state with no intermediates, is also most likely an octamer, as must be at least a component of the noisy P state. Analysis of the asymmetry of chemical modification and electrical recordings with cWza peptides with hydrophilic extensions further revealed that the peptides are arranged in parallel with their N termini on the cis side of the membrane, to which the peptides are added, and their C termini on the trans side. We also constructed a candelabrum-like molecule comprising γ-cyclodextrin connected to eight cWza-S355C D4 peptides through disulfide bonds. In accord with the structure deduced for the cWza pore and the assembly model, this construct inserted into bilayers spontaneously, and by virtue of its structure, C terminus first. Upon cleavage of the disulfide bonds, a high-conductance pore remained permanently open in the bilayer

with properties similar, but not identical, to the H state formed directly from cWza peptides.

Our observation that amphipathic α helices can assemble to form discrete membrane-spanning pores with stable and reproducible conductance properties is remarkable and relevant to other fields. For example, despite considerable effort, it has been difficult to define the assembly mechanisms and structures of the pore-forming states of certain classes of antimicrobial peptides[40-42]. While these pores are invariably heterogeneous, the cWza peptide pore may exemplify one of the several states. Further, the interconversion of the L and H states reported here may contribute to an understanding of how mechanosensitive channels gate in response to changes in membrane tension[32,33,43,44].

Applications for nanopores continue to emerge in biotechnology and medicine[17]. Our studies with short, Wza-based peptides open up the possibility of using engineered or *de novo* designed α-helix barrels as components of single-molecule sensors or sequencers[20] **(Supplementary Fig. S19)**. Further unnatural amino acids can be incorporated by chemical synthesis into the peptides, which might then be used for single-molecule chemistry[45] and other biotechnological applications. Engineered α-helix barrels may also find applications in medicine. For example, designed peptides might be valuable as antimicrobial agents[46,47]. Similarly, pore-forming peptides might be targeted to cancer cells[48,49]. Our future studies will focus on the engineering of peptides, for example to control the number of helices, to create heteromeric structures[18] and to span two bilayers[50].

Methods

Electrical recordings

Planar lipid bilayer recordings were carried out by using bilayers of 1,2-diphytanoyl-*sn*-glycero-3-phosphocholine (DPhPC, Avanti Polar Lipids) formed across an aperture (~50 µm in diameter) in a 25-µm thick polytetrafluoroethylene (Teflon) film (Goodfellow, Cambridge), which separated the apparatus into cis and trans compartments (1 mL each)[51]. Bilayers were formed by first pre-treating the aperture with hexadecane in n-pentane (1 µL, 10 mg mL^{-1}) on each side. Both compartments were then filled with the electrolyte solution (1 M KCl, 10 mM HEPES, pH 7.4) and DPhPC in n-pentane (5 µL, 5 mg mL^{-1}) was added to both sides whereupon the solvent evaporated. A bilayer was formed when the electrolyte was raised bringing the two lipid surface monolayers together at the aperture. Peptides were always added to the cis compartment. cWza pores were formed by adding a solution of the peptide under examination in 0.05% DDM (1 µL, 100 µg mL^{-1}) to the cis compartment with stirring under an applied potential of +100 to +200 mV. The cis compartment was connected to the grounded electrode and the trans compartment was connected to the working electrode. A potential difference was applied through a pair of Ag/AgCl electrodes, set in 2% agarose containing 3.0 M KCl. The current was amplified by using an Axopatch 200B amplifier, digitized with a Digidata 1440A A/D converter and recorded with the pClamp 10.3 acquisition software (Molecular Devices,CA) with a low-pass filter frequency of 2 kHz and a sampling frequency of 10 kHz. Cyclodextrin blocking current signals were filtered at 10 kHz and sampled at 50 kHz. The data were analyzed and prepared for presentation with pClamp (version 10.3, Molecular Devices, CA) and Origin 9.0.

Peptide synthesis

Peptides were synthesized by the Fmoc solid-phase peptide synthesis method with a CEM Liberty Blue automated synthesizer with inline UV monitoring. N,N'-diisopropylcarbodiimide/1-hydroxybenzotriazole was used for activation. All peptides were produced as the C-terminal amide on the solid support and N-terminally acetylated by N,N-diisopropylethylamine (4.5 eq.) and acetic anhydride (3 eq.) in N,N-dimethylformamide for 30 min. Fmoc-Ile-Thr($\psi^{Me,Mepro}$)-OH was used at the I361-T362 position for all peptides. Cleavage from the solid support was performed with a mixture of trifluoroacetic acid (TFA)/triisopropylsilane/water (90/5/5, v/v/v). Additional 5% ethanedithiol was used for all Cys-containing peptides. The cleavage solution was reduced in volume to ~1 mL by using a flow of nitrogen. Diethyl ether (45 mL) was added to obtain a precipitate that was recovered by centrifugation and redissolved in acetonitrile/water (1/1) before freeze-drying, to yield the crude peptide. Peptides were purified by reversed-phase HPLC, with a gradient of 20 to 80% acetonitrile in water (each containing 0.1% TFA) over 45 min on Vydac ® TP C18 column (10 µm particle, 22 × 250 mm). Fractions containing pure peptide were identified by analytical HPLC and MALDI-TOF mass spectrometry. Analytical HPLC was performed with a Jasco 2000 series HPLC system with a Phenomenex 'Kinetex' C18 column (5 µm particle, 4.6 mm × 100 mm), monitored at 220. The gradient was 20 to 80% acetonitrile/water (each containing 0.1% TFA) over 16 min. MALDI-TOF mass spectra were obtained on a Bruker UltraFlex MALDI-TOF mass spectrometer in positive-ion reflector mode. Peptide solutions were spotted on a ground steel target plate with dihydroxybenzoic acid as the matrix. Calibration was conducted using the 'nearest neighbor' method, with Bruker Peptide Calibration Standard II as the reference masses.

Circular dichroism spectroscopy

Circular dichroism spectra were obtained using JASCO J-810 or J-815 spectropolarimeters fitted with Peltier temperature controllers (Jasco UK). Peptide samples were prepared as 50 or 22 µM solutions in phosphate buffered saline (PBS, 8.2 mM sodium phosphate, 1.8 mM potassium phosphate, 137 mM sodium chloride, 2.7 mM potassium chloride at pH 7.4) with 1% DDM or 0.35% C8E5. Spectra were collected using a 1 mm path length quartz cuvette at 20 °C. For each dataset (in deg), baselines from the same buffer and cuvette were subtracted, and then data points were normalized for amide bond concentration and path length to give mean residue ellipticity (MRE; deg cm^2 $dmol^{-1}$ res^{-1}).

Analytical ultracentrifugation:

Sedimentation equilibrium experiments by analytical ultracentrifugation were performed with a Beckman Optima XL-I or XL-A analytical ultracentrifuge using an An-50 Ti or An-60 Ti rotor (Beckman-Coulter). Samples were prepared in PBS containing 0.35% C8E5 with peptide concentrations in the range of 20 – 40 µM and centrifuged at a speed in the range of 36 to 42 krpm. Datasets were fitted to monomer-dimer equilibrium models by using Ultrascan II (http:/www.ultrascan.uthscsa.edu). The partial specific volume for each of the peptides and the buffer density were calculated using Sednterp (http://sednterp.unh.edu/).

Acknowledgements

The authors acknowledge a BBSRC grant (BB/J009784/1) and the ERC (340764) for financial support. DNW holds a Royal Society Wolfson Research Merit Award.

Author contributions

KRM performed and analyzed current recordings. AN synthesized peptides and determined their biophysical properties. LK produced Wza protein and synthesized cyclodextrin derivatives. AN and ART performed molecular modeling. AN and RBS performed molecular dynamics simulations. KRM, AN, DNW, and HB designed experiments and wrote the paper.

References

1. Woolfson, D.N. The design of coiled-coil structures and assemblies. *Adv. Protein Chem.* **70,** 79-112 (2005).

2. Woolfson, D.N. et al. De novo protein design: how do we expand into the universe of possible protein structures? *Curr. Opin. Struct. Biol.* **33**, 16-26 (2015).

3. Woolfson, D.N., Bartlett, G.J., Bruning, M. & Thomson, A.R. New currency for old rope: from coiled-coil assemblies to alpha-helical barrels. *Curr. Opin. Struct. Biol.* **22,** 432-41 (2012).

4. Lear, J.D., Wasserman, Z.R. & DeGrado, W.F. Synthetic amphiphilic peptide models for protein ion channels. *Science* **240,** 1177-81 (1988).

5. Joh, N.H. et al. De novo design of a transmembrane Zn^{2+} -transporting four-helix bundle. *Science* **346,** 1520-4 (2014).

6. Franceschini, L., Soskine, M., Biesemans, A. & Maglia, G. A nanopore machine promotes the vectorial transport of DNA across membranes. *Nat. Commun.* **4,** 2415 (2013).

7. Bayley, H. Membrane-protein structure: Piercing insights. *Nature* **459,** 651-2 (2009).

8. Dong, C. et al. Wza the translocon for E. coli capsular polysaccharides defines a new class of membrane protein. *Nature* **444,** 226-9 (2006).

9. Kong, L. et al. Single-molecule interrogation of a bacterial sugar transporter allows the discovery of an extracellular inhibitor. *Nat. Chem.* **5,** 651-9 (2013).

10. Soskine, M. et al. An engineered ClyA nanopore detects folded target proteins by selective external association and pore entry. *Nano Lett.* **12,** 4895-900 (2012).

11. Soskine, M., Biesemans, A., De Maeyer, M. & Maglia, G. Tuning the size and properties of ClyA nanopores assisted by directed evolution. *J. Am. Chem. Soc.* **135,** 13456-63 (2013).

12. Tanaka, K., Caaveiro, J.M., Morante, K., Gonzalez-Manas, J.M. & Tsumoto, K. Structural basis for self-assembly of a cytolytic pore lined by protein and lipid. *Nat. Commun.* **6,** 6337 (2015).

13. Zaccai, N.R. et al. A de novo peptide hexamer with a mutable channel. *Nat. Chem. Biol.* **7,** 935-41 (2011).

14. Thomson, A.R. et al. Computational design of water-soluble alpha-helical barrels. *Science* **346,** 485-8 (2014).

15. Bayley, H. Designed membrane channels and pores. *Curr. Opin. Biotechnol.* **10,** 94-103 (1999).

16. Bayley, H. & Jayasinghe, L. Functional engineered channels and pores (Review). *Mol. Membr. Biol.* **21**, 209-20 (2004).

17. Majd, S. et al. Applications of biological pores in nanomedicine, sensing, and nanoelectronics. *Curr. Opin. Biotechnol.* **21,** 439-76 (2010).

18. Braha, O. et al. Designed protein pores as components for biosensors. *Chem. Biol.* **4,** 497-505 (1997).

19. Bayley, H. & Cremer, P.S. Stochastic sensors inspired by biology. *Nature* **413,** 226-30 (2001).

20. Bayley, H. Nanopore sequencing: from imagination to reality. *Clin. Chem.* **61,** 25-31 (2015).

21. Jain, M. et al. Improved data analysis for the MinION nanopore sequencer. *Nat. Methods* **12,** 351-6 (2015).

22. Song, L. et al. Structure of staphylococcal alpha-hemolysin, a heptameric transmembrane pore. *Science* **274,** 1859-66 (1996).

23. Gu, L.Q., Braha, O., Conlan, S., Cheley, S. & Bayley, H. Stochastic sensing of organic analytes by a pore-forming protein containing a molecular adapter. *Nature* **398,** 686-90 (1999).

24. Banerjee, A. et al. Molecular bases of cyclodextrin adapter interactions with engineered protein nanopores. *Proc. Natl. Acad. Sci. U S A* **107,** 8165-70 (2010).

25. Walshaw, J. & Woolfson, D.N. Socket: a program for identifying and analysing coiled-coil motifs within protein structures. *J. Mol. Biol.* **307,** 1427-50 (2001).

26. van den Berg, B., Prathyusha Bhamidimarri, S., Dahyabhai Prajapati, J., Kleinekathofer, U. & Winterhalter, M. Outer-membrane translocation of bulky small molecules by passive diffusion. *Proc. Natl. Acad. Sci. U S A* **112,** E2991-9 (2015).

27. Doyle, D.A. et al. The structure of the potassium channel: molecular basis of K+ conduction and selectivity. *Science* **280,** 69-77 (1998).

28. Mueller, M., Grauschopf, U., Maier, T., Glockshuber, R. & Ban, N. The structure of a cytolytic alpha-helical toxin pore reveals its assembly mechanism. *Nature* **459,** 726-30 (2009).

29. Miles, G., Movileanu, L. & Bayley, H. Subunit composition of a bicomponent toxin: staphylococcal leukocidin forms an octameric transmembrane pore. *Protein Sci* **11**, 894-902 (2002).

30. Smart, O.S., Breed, J., Smith, G.R. & Sansom, M.S. A novel method for structure-based prediction of ion channel conductance properties. *Biophys. J.* **72,** 1109-26 (1997).

31. Sukharev, S., Betanzos, M., Chiang, C.S. & Guy, H.R. The gating mechanism of the large mechanosensitive channel MscL. *Nature* **409,** 720-4 (2001).

32. Wang, Y. et al. Single molecule FRET reveals pore size and opening mechanism of a mechano-sensitive ion channel. *Elife* **3,** e01834 (2014).

33. Pliotas, C. et al. The role of lipids in mechanosensation. *Nat. Struct. Mol. Biol.* (2015).

34. Walker, B., Krishnasastry, M., Zorn, L. & Bayley, H. Assembly of the oligomeric membrane pore formed by Staphylococcal alpha-hemolysin examined by truncation mutagenesis*. J. Biol. Chem.* **267,** 21782-6 (1992).

35. Walker, B., Braha, O., Cheley, S. & Bayley, H. An intermediate in the assembly of a pore-forming protein trapped with a genetically-engineered switch. *Chem. Biol.* **2,** 99-105 (1995).

36. Dunstone, M.A. & Tweten, R.K. Packing a punch: the mechanism of pore formation by cholesterol dependent cytolysins and membrane attack complex/perforin-like proteins. *Curr. Opin. Struct. Biol.* **22,** 342-9 (2012).

37. Leung, C. et al. Stepwise visualization of membrane pore formation by suilysin, a bacterial cholesterol-dependent cytolysin. *Elife* **3,** e04247 (2014).

38. Stoddart, D. et al. Functional truncated membrane pores. *Proc. Natl. Acad. Sci. U S A* **111,** 2425-30 (2014).

39. Karginov, V.A. Cyclodextrin derivatives as anti-infectives. *Curr. Opin. Pharmacol.* **13,** 717-25 (2013).

40. Brogden, K.A. Antimicrobial peptides: pore formers or metabolic inhibitors in bacteria? *Nat. Rev. Microbiol*. **3,** 238-50 (2005).

41. Cirac, A.D. et al. The molecular basis for antimicrobial activity of pore-forming cyclic peptides. *Biophys. J.* **100,** 2422-31 (2011).

42. Song, C. et al. Crystal structure and functional mechanism of a human antimicrobial membrane channel. *Proc. Natl. Acad. Sci. U S A* **110,** 4586-91 (2013).

43. Haswell, E.S., Phillips, R. & Rees, D.C. Mechanosensitive channels: what can they do and how do they do it? *Structure* **19,** 1356-69 (2011).

44. Naismith, J.H. & Booth, I.R. Bacterial mechanosensitive channels--MscS: evolution's solution to creating sensitivity in function. *Annu. Rev. Biophys.* **41,** 157-77 (2012).

45. Lee, J. & Bayley, H. Semisynthetic protein nanoreactor for single-molecule chemistry. *Proc. Natl. Acad. Sci. U S A* **112**, 13768-73 (2015).

46. Fernandez-Lopez, S. et al. Antibacterial agents based on the cyclic D,L-alpha-peptide architecture. *Nature* **412,** 452-5 (2001).

47. Fjell, C.D., Hiss, J.A., Hancock, R.E. & Schneider, G. Designing antimicrobial peptides: form follows function. *Nat. Rev. Drug. Discov.* **11,** 37-51 (2012).

48. Hoskin, D.W. & Ramamoorthy, A. Studies on anticancer activities of antimicrobial peptides. *Biochim. Biophys. Acta* **1778,** 357-75 (2008).

49. Gaspar, D., Veiga, A.S. & Castanho, M.A. From antimicrobial to anticancer peptides. A review. *Front. Microbiol.* **4,** 294 (2013).

50. Mantri, S., Sapra, K.T., Cheley, S., Sharp, T.H. & Bayley, H. An engineered dimeric protein pore that spans adjacent lipid bilayers. *Nature communications* **4**, 1725 (2013).

51. Gutsmann, T., Heimburg, T., Keyser, U., Mahendran, K.R. & Winterhalter, M. Protein reconstitution into freestanding planar lipid membranes for electrophysiological characterization. *Nat. Protoc.* **10,** 188-98 (2015).

Figure Legends

Figure 1: Structure of *Escherichia coli* Wza, peptide design and electrical properties of the cWza pore.

a) Structure of native *Escherichia coli* Wza (PDB: 2J58). **b)** Structure of the Wza D4 domain. **c)** WebLogo (http://weblogo.berkeley.edu/) representation of a BLAST search for the Wza D4 domain (top) showing the consensus Wza peptide (cWza) sequence (below). **d)** Electrical recording of multiple insertions of cWza peptide pores into a planar bilayer at +100 mV. Each step represents the appearance of an L state. **e)** Appearance of the precursor state P followed by conversion to the low conductance pore L at +100 mV. The P state can also form reversibly **(Supplementary Fig. S17)**. **f)** Histogram of the unitary conductance of L events at +100 mV. The mean unitary conductance was obtained by fitting the distribution to a Gaussian (n = 110). **g)** Interconversion of an L state and an H state at +200 mV. **h)** Histogram of the unitary conductance of H events at +200 mV. The mean unitary conductance was obtained by fitting the distribution to a Gaussian (n =100). **i)** Conversion of an L state to the P state followed by closure at +100 mV. Electrolyte: 1 M KCl, 10 mM HEPES, pH 7.4. The current signals were filtered at 2 kHz and sampled at 10 kHz. In all experiments, cWza peptide pores were formed by adding the peptide to the cis compartment.

Figure 2: Electrical properties of mutant cWza pores.

a) Structural models of cWza-K375C peptides with two helices facing each other. The D4 α-helix barrel in the native Wza crystal structure (PDB: 2J58) was used as a template. **b)** P state of a cWza-K375C pore and its conversion to the L state at +100 mV. **c)** Histogram of the unitary conductance values of cWza-K375C L events at

+100 mV. The mean unitary conductance was obtained by fitting the distribution to a Gaussian (n = 100). **d)** H state of a cWza-K375C pore and conversion of the L state at +200 mV. **e)** Histogram of the unitary conductance values of cWza-K375C H events at +200 mV. The mean unitary conductance was obtained by fitting the distribution to a Gaussian (n = 100). **f)** L state of a cWza-K375C pore and closure via the P state at +100 mV. **g)** Structural models of cWza-Y373C peptides with two helices facing each other. The D4 α-helix barrel in the native Wza crystal structure (PDB: 2J58) was used as a template. **h)** P states of the cWza-Y373C pore and conversion to the H state at +100 mV. **i)** Histogram of the unitary conductance values of cWza-Y373C H events at +100 mV. The mean unitary conductance was obtained by fitting the distribution to a Gaussian (n = 100). **j)** Single cWza-Y373C pore at +200 mV. **k)** I-V curve obtained from a single cWza-Y373C pore. Electrolyte: 1 M KCl, 10 mM HEPES, pH 7.4. The current signals were filtered at 2 kHz and sampled at 10 kHz.

Figure 3: Interaction of cWza peptide pores with cationic cyclodextrins.
a) Structure of am_8γCD, interaction of the cWza-K375C H state with am_8γCD (100 µM, trans) at +50 mV and +150 mV, and a plot of k_{off} versus the applied potential (n = 3). **b)** Structure of am_6αCD, interaction of the cWza-K375C H state with am_6αCD (100 µM, trans) at +50 mV and +150 mV, and a plot of k_{off} versus the applied potential (n = 3). **c)** Competitive interaction of the cWza-K375C H state with am_6αCD and am_8γCD (both 100 µM, trans) at +50 mV. The current signals were filtered at 10 kHz and sampled at 50 kHz. **d)** Interaction of the cWza-Y373C H state with am_8γCD (100 µM, trans) at +50 mV and +100 mV, and with am_6αCD (100 µM, trans) at +100

mV. The current signals were filtered at 2 kHz and sampled at 10 kHz. Electrolyte: 1 M KCl, 10 mM HEPES, pH 7.4.

Figure 4: Orientation and stoichiometry of the cWza-Y373C pore

a) Reaction of 1 mM MePEG-OPSS-5k (trans) with the cWza-Y373C H state at +50 mV. The structures of the PEG reagents are shown in **(Supplementary Fig. S12)**. **b)** Subsequent addition of 10 mM DTT (trans) resulting in the cleavage of PEG chains from the pore. **c)** Reaction of 1 mM MePEG-OPSS-5k (cis) with the cWza-Y373C H state at +50 mV. Pore blockade was not observed. **d)** It was deduced that cWza-Y373C added to the cis compartment formed a stable pore with all the peptides oriented so that the C termini faced the trans compartment. **e)** Reaction of 1 mM MePEG-OPSS-1k (trans) with the cWza-Y373C pore at +50 mV. Inset: histogram showing the number of current steps seen after the addition of 1 mM MePEG-OPSS-1k (trans) to individual cWza-Y375C pores. **f)** Reaction of 1 mM MePEG-OPSS-1k (cis) with the cWza-Y373C pore at +50 mV. The displayed current signals (**a-f**) were digitally filtered at 200 Hz using an 8-pole Bessel digital filter **g)** Formation of a K4-cWza-Y373C pore at +100 mV. **h)** The cWza-Y373C-K4 pore fluctuates between different conductance states at +100 mV. The current signals (**g, h**) were filtered at 2 kHz and sampled at 10 kHz. Electrolyte: 1 M KCl, 10 mM HEPES, pH 7.4.

Figure 5: The cyclodextrin-templated barrel and its electrical properties.

a) The γ-cyclodextrin $(PDPam)_8$γCD was coupled to cWza-S355C through disulfide bonds. The structure of the fully derivatized cyclodextrin, $(cWza\text{-}S355C\text{-}TPam)_8$γCD, is based on the D4 domain in the native Wza crystal structure (PDB: 2J58). **b)** The peptide-cyclodextrin conjugates, peptide and protein markers (M) were run on an

SDS-PAGE gel. The arrow indicates the presumed fully derivatized (cWza-S355C-TPam)$_8$γCD. **c)** Electrical recording of a single (cWza-S355C-TPam)$_8$γCD pore. **d)** Single (cWza-S355C-TPam)$_8$γCD pore after treatment with 10 mM DTT (cis). For display, the current signals (**c, d**) were digitally filtered at 500 Hz using an 8-pole Bessel digital filter.

Figure 6: Model for membrane insertion and pore formation by cWza peptides. The cWza peptide binds to the membrane to form a precursor state P, which converts to a low-conductance state, L. At high potentials L is converted to a high-conductance state H, which can be blocked by cationic cyclodextrins. The pore can close, via the P state, by reversal of the assembly pathway. The L and H states most likely comprise 8 helices (see the main text), while the structure of the noisy P state is likely to be less stable but with an octameric component that transitions into the L state. The structure of the H state is based on that of the D4 domain in native Wza. The structure of the L state is a coiled-coil octamer with dimensions that reflect the lower conductance of this state **(Supplementary Fig. S1)**.

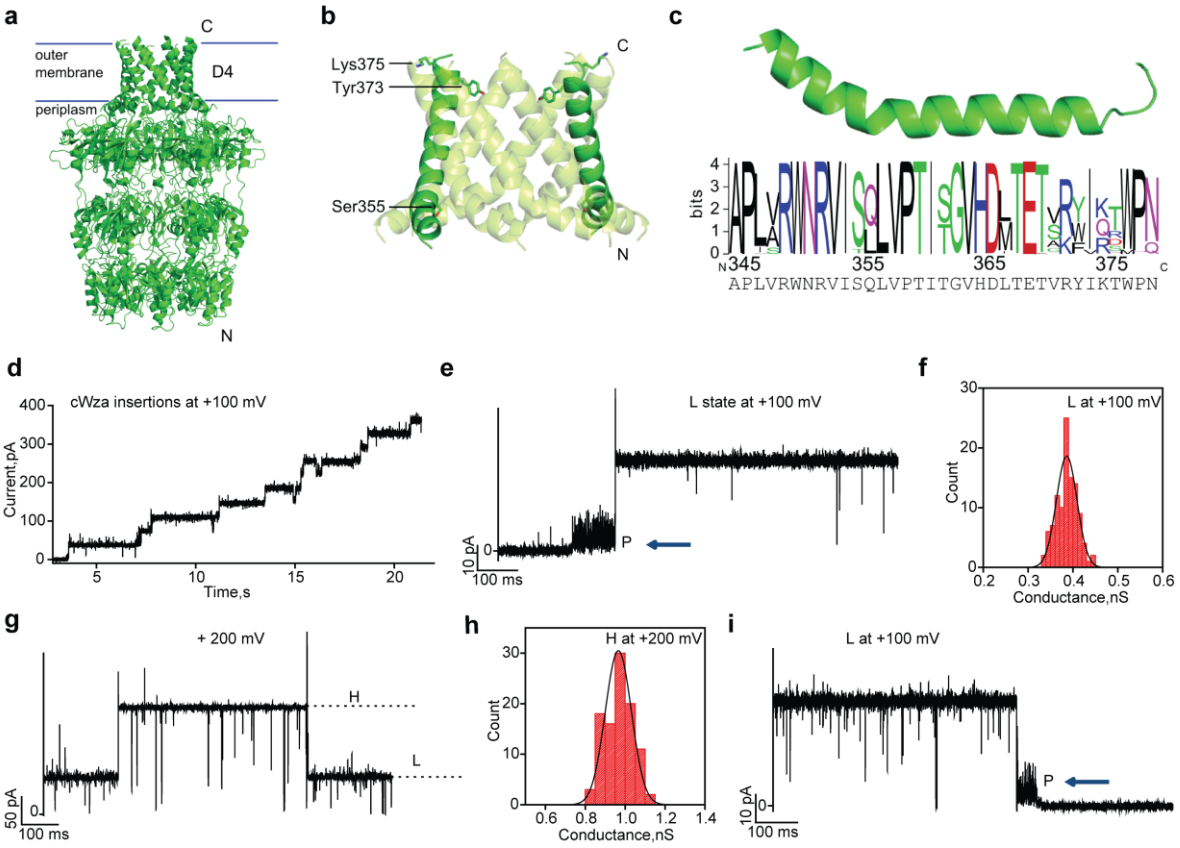
a
C
outer membrane
D4
periplasm
N
b
Lys375
Tyr373
Ser355
C
N
c
bits
APLVRWNRVISQLVPTITGVHDLTETVRYIKTWPN
d
cWza insertions at +100 mV
Current,pA
Time,s
e
L state at +100 mV
P
10 pA
100 ms
f
L at +100 mV
Count
Conductance,nS
g
+ 200 mV
H
L
50 pA
100 ms
h
H at +200 mV
Count
Conductance,nS
i
L at +100 mV
P
10 pA
100 ms

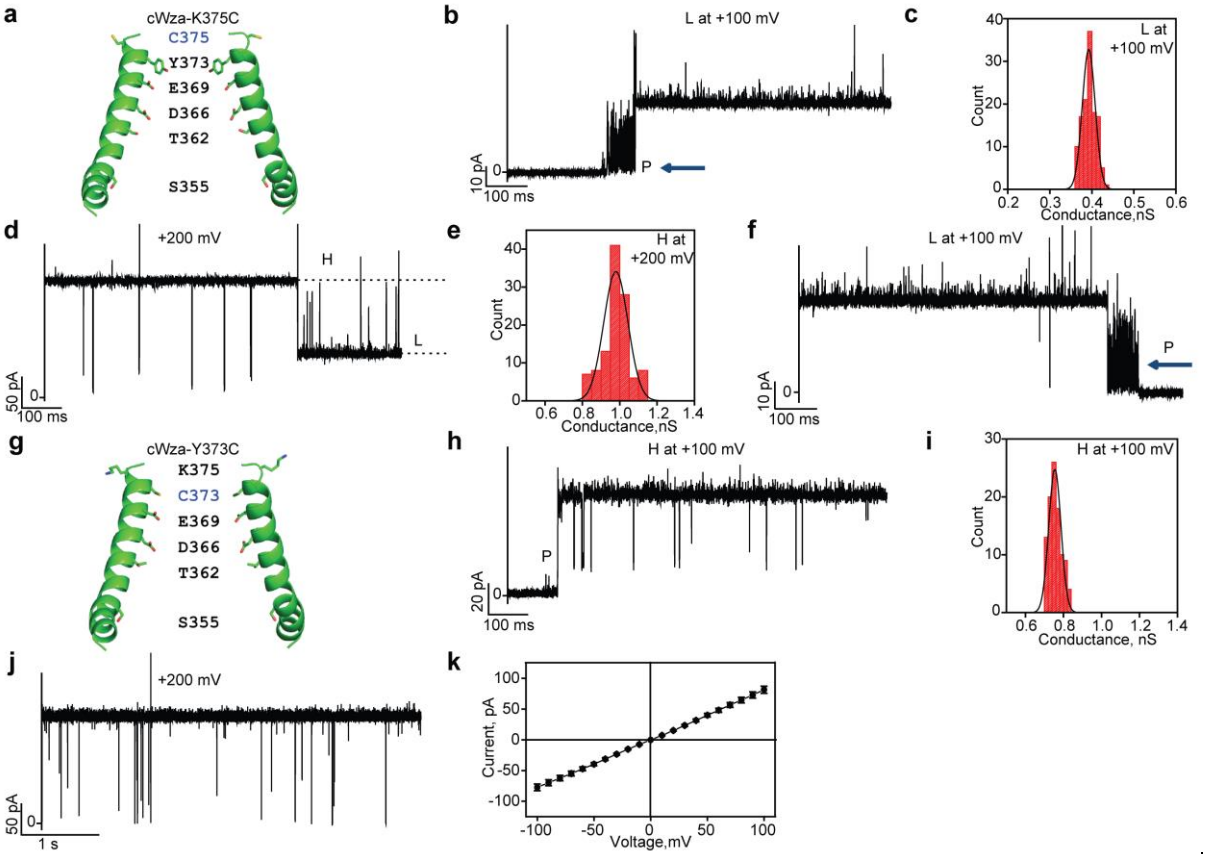
a
cWza-K375C
C375
Y373
E369
D366
T362
S355
b
L at +100 mV
10 pA
0
100 ms
P
c
L at
+100 mV
Count
Conductance,nS
d
+200 mV
H
L
50 pA
0
100 ms
e
H at
+200 mV
Count
Conductance,nS
f
L at +100 mV
P
10 pA
0
100 ms
g
cWza-Y373C
K375
C373
E369
D366
T362
S355
h
H at +100 mV
P
20 pA
0
100 ms
i
H at +100 mV
Count
Conductance, nS
j
+200 mV
50 pA
0
1 s
k
Current, pA
Voltage,mV

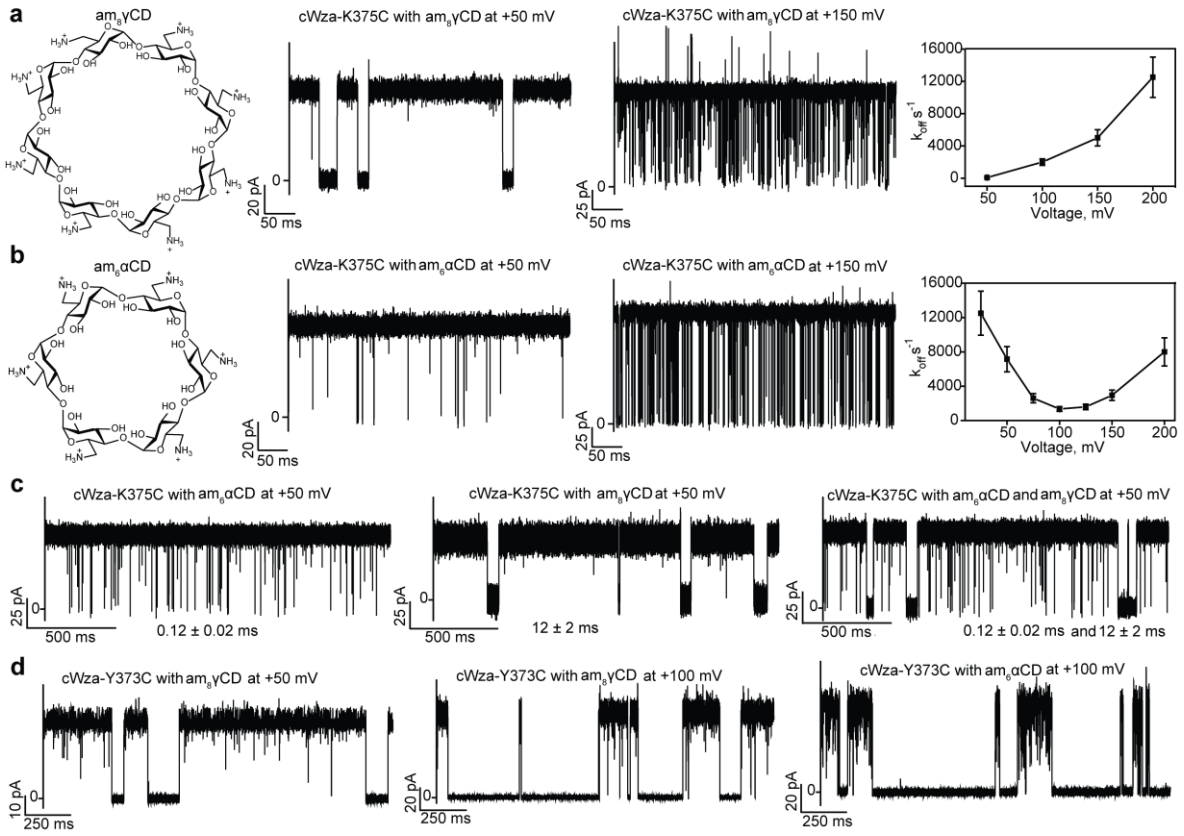
a
am8γCD
cWza-K375C with am8γCD at +50 mV
cWza-K375C with am8γCD at +150 mV
20 pA
25 pA
50 ms
koff s-1
Voltage, mV
b
am6αCD
cWza-K375C with am6αCD at +50 mV
cWza-K375C with am6αCD at +150 mV
c
cWza-K375C with am6αCD at +50 mV
cWza-K375C with am8γCD at +50 mV
cWza-K375C with am6αCD and am8γCD at +50 mV
500 ms
0.12 ± 0.02 ms
12 ± 2 ms
0.12 ± 0.02 ms and 12 ± 2 ms
d
cWza-Y373C with am8γCD at +50 mV
cWza-Y373C with am8γCD at +100 mV
cWza-Y373C with am6αCD at +100 mV
10 pA
250 ms

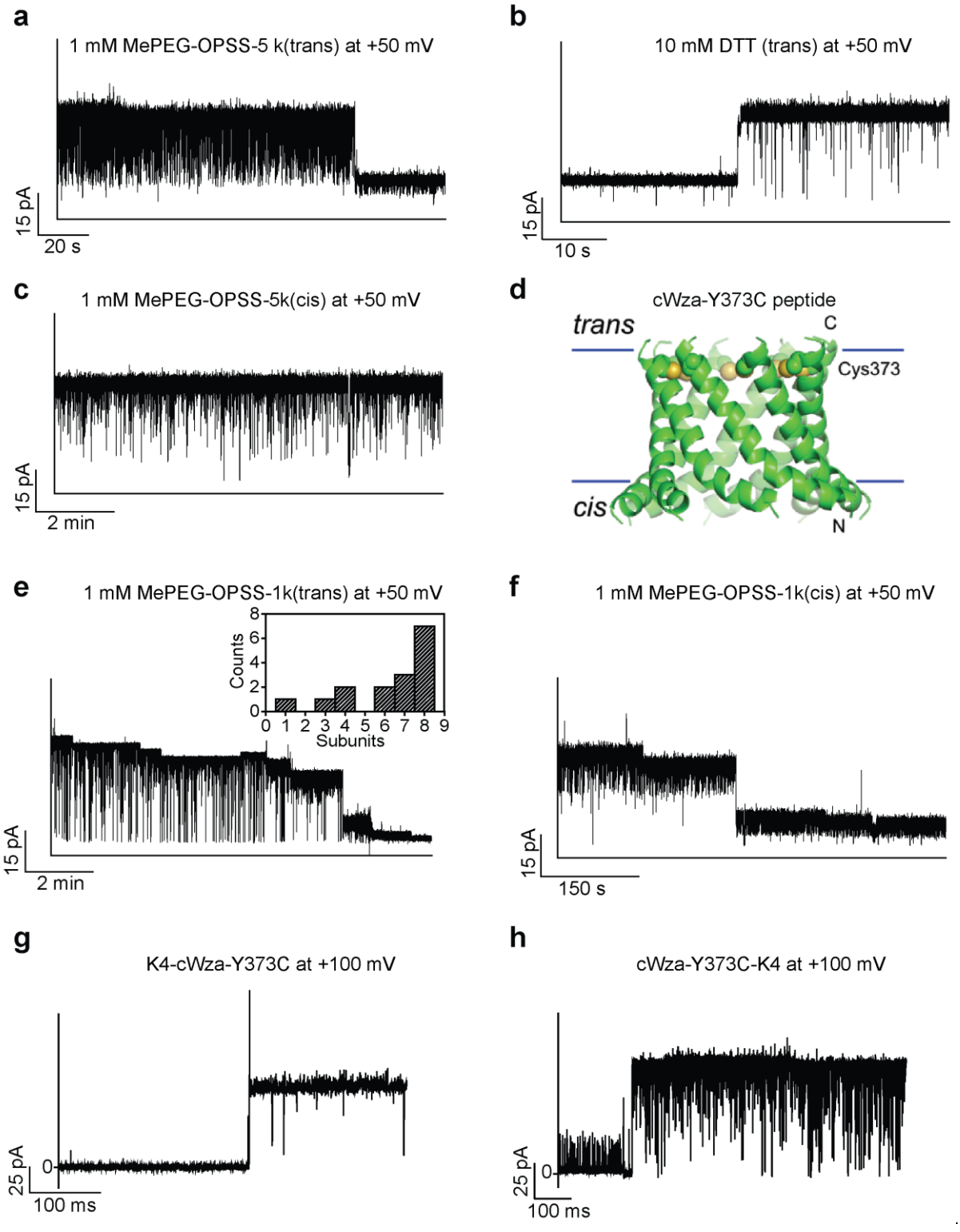
a
1 mM MePEG-OPSS-5 k(trans) at +50 mV
15 pA
20 s
b
10 mM DTT (trans) at +50 mV
15 pA
10 s
c
1 mM MePEG-OPSS-5k(cis) at +50 mV
15 pA
2 min
d
cWza-Y373C peptide
trans
C
Cys373
cis
N
e
1 mM MePEG-OPSS-1k(trans) at +50 mV
Counts
Subunits
15 pA
2 min
f
1 mM MePEG-OPSS-1k(cis) at +50 mV
15 pA
150 s
g
K4-cWza-Y373C at +100 mV
25 pA
0
100 ms
h
cWza-Y373C-K4 at +100 mV
25 pA
0
100 ms

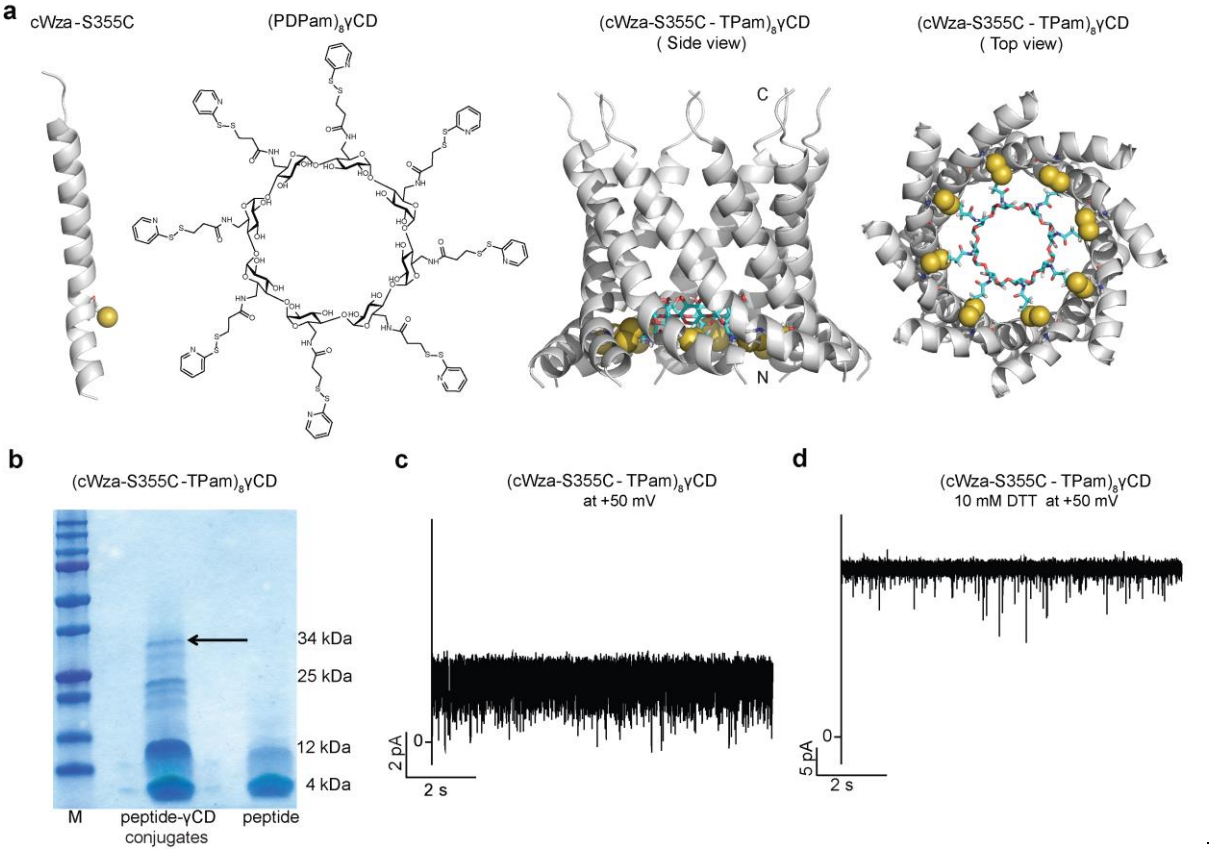
a
cWza-S355C
(PDPam)8γCD
(cWza-S355C - TPam)8γCD
(Side view)
(cWza-S355C - TPam)8γCD
(Top view)
C
N
b
(cWza-S355C-TPam)8γCD
34 kDa
25 kDa
12 kDa
4 kDa
M
peptide-γCD
conjugates
peptide
c
(cWza-S355C - TPam)8γCD
at +50 mV
2 pA
0
2 s
d
(cWza-S355C - TPam)8γCD
10 mM DTT at +50 mV
5 pA
0
2 s

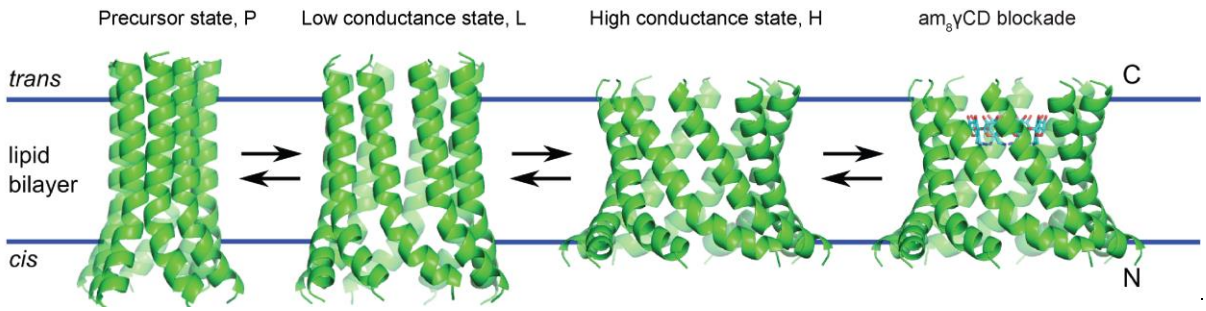
Precursor state, P
Low conductance state, L
High conductance state, H
am8γCD blockade
trans
lipid
bilayer
cis
C
N